Comments on "The Gulf Stream Convergence Zone in the Time-Mean Winds"

Riwal Plougonven, Alexis Foussard, Guillaume Lapeyre

Comment on 'The Gulf Stream Convergence Zone in the time-mean winds'

Riwal Plougonven*

Laboratoire de Météorologie Dynamique/IPSL, Ecole polytechnique, Université Paris Saclay, France

Alexis Foussard

Laboratoire de Météorologie Dynamique/IPSL, Ecole Normale Supérieure, PSL Research University, France

Guillaume Lapeyre

Laboratoire de Météorologie Dynamique/IPSL, Ecole Normale Supérieure, PSL Research University, France

Corresponding author address: LMD/IPSL, Ecole Polytechnique, Palaiseau, France.

E-mail: riwal.plougonven@polytechnique.org

ABSTRACT

In a recent study, O'Neill and co-authors have analysed the divergence of surface winds above the northwest Atlantic. In the time-mean, a band of convergence is found, overlying the Southern flanck of the Gulf Stream. To quantify the impact of storms, they have averaged divergence conditionally on the absence of rain, or have averaged divergence excluding extreme values. In the resulting averages, divergence is found to be positive nearly everywhere, hence the band of convergence is no longer present as convergence. O'Neill and coauthors claim that this absence of convergence in these averages allows to draw conclusions about the mechanisms underlying the atmospheric response to the Gulf Stream. We show that this absence of negative values results from the correlation between rain and divergence: averaging divergence conditionally on the absence of rain automatically implies a positive shift. In consequence, we argue that these statistics do not allow conclusions on the underlying mechanisms, but have the merit of highlighting the essential role of storms in shaping the divergence field in instantaneous fields.

1. Introduction

O'Neill et al. (2017) have recently presented a detailed analysis on the relation between surface divergence and the underlying Sea Surface Temperature (SST) anomalies, drawing from a ten-year record of satellite measurements and from a one-year simulation with a regional model. Their focus was on the relation between the time-mean surface divergence and the fluctuations associated to passing storms. Indeed, the time-mean divergence of surface winds (or of surface stress on the ocean) has been abundantly studied in the past decade, showing a conspicuous relation to SST (Small et al. (2008); Bryan et al. (2010) and references therein). In particular, Minobe et al. (2008) convincingly showed that there is convergence on the warm flank of the Gulf Stream and divergence on the cold flank. Yet, this time-mean divergence is of order $10^{-5}\,\mathrm{s}^{-1}$, i.e. one order of magnitude weaker than the maximum instantaneous values found in the divergence field (of order $10^{-4}\,\mathrm{s}^{-1}$). These extreme values of surface divergence are often negative values (i.e. convergence) tied to surface fronts and the associated resulting convection (e.g. Figure 4 of O'Neill et al. (2017)).

O'Neill et al. (2017) (hereafter ON17) have used different approaches and filters to isolate the contribution of storms to the time-mean signature in divergence. Their systematic analysis provides a novel and valuable outlook on an important aspect of the effect of SST on atmospheric dynamics. Indeed, different mechanisms have been proposed to explain the relation between SST and the overlying winds. On the one hand, the vertical-momentum mixing mechanism relies on the vertical stability of atmospheric boundary layer over SST anomalies (Businger and Shaw 1984; Hayes et al. 1989; Chelton et al. 2004). On the other hand, a pressure adjustment mechanism relies on the hypothesis that the boundary layer is in an Ekman-like balance (Lindzen and Nigam 1987; Feliks et al. 2004; Minobe et al. 2008; Lambaerts et al. 2013).

However the related studies have often focused on the time-mean fields and the interplay of different mechanisms in instantaneous complex flow fields remains unclear.

This problem falls in a broader category of problems common in geophysical fluid dynamics, in which a weak time-averaged signal is dwarfed in any instantaneous flow field by temporary fluctuations. As other examples, one may think of the Hadley circulation, mean currents in the ocean which are often dominated by the mesoscale eddy field, or the Brewer-Dobson circulation (Butchart 2014), for which the ascending motion in the Tropics can only be indirectly inferred, because the associated vertical velocities are dwarfed by the signatures of equatorial waves in any snapshot of the flow field.

We wish to build on the analysis of ON17 and to point out an aspect of the method used in their paper that needs to be emphasized. Indeed, part of the conclusions put forward by ON17 relies on the computation of conditional averages of different fields. However, part of the interpretation of these statistics is not justified. Specifically, they claim that, because of the absence of convergence in 'rain-free' conditions (occurring between 80 and 90% of the time, see figure 2 of ON17), an 'Ekman-Balanced mass adjustment' mechanism (EBMA) cannot be at work. The underlying premise is that this mechanism should be 'persistent', and therefore be present even when averaging over a subset of times, especially a large subset.

The present comment aims merely to point out that conditional averages and other similar filters that are considered by ON17 introduce a bias, because the variable used for the condition is strongly correlated to the variable that is averaged. In the present case, it is not the sign of the averaged divergence that is meaningful, but rather its spatial variations. With that in mind, there is no longer a straightforward transition from ON17's results to an interpretation in terms of mechanisms. Nonetheless, we acknowledge that the study of ON17 has the merit of unveiling

the possible role of synoptic storms in shaping the different mechanisms at work in instantaneous winds.

In section 2, a toy model is proposed to illustrate the difficulty in diagnosing the behavior of the marine atmospheric boundary layer (MABL) and storms in instantaneous or time-mean winds. An idealized simulation of storm tracks carried out with the WRF model is then investigated in section 3, both to further illustrate and confirm the statements of section 2, but also to explore how the time-mean divergence may result from a combination of mechanisms. Implications and directions for further research are discussed in section 4.

2. A toy model for illustrating conditional averages

In order to clarify the interpretation of the observations and model simulations carried out by ON17, we propose to consider a very simplified model.

a. On the sign of the average divergence

Many of the conclusions of ON17 come from the fact that the conspicuous band of *convergence* on the Southern flank of the Gulf Stream vanishes when divergence is averaged for rain-free conditions only (their figure 1b), or when other filters retaining rain events are used (figure 5b and 8b). It is the disappearance of the negative values (in green with their colorbar) which they emphasize. ON17 deduce *'that the existence of the Gulf Stream Convergence Zone in the time-mean winds owes its existence to extreme storm convergences, since removing a relatively small number of data points associated with storms removes the time-mean convergence.*' (ON17, end of section 3f, p2397). This line of reasoning bears a fundamental flaw as the conclusions of ON17 are mainly based on the *sign* of the rain-free time-mean convergence. In fact, it can be shown that any conditional average (here, rain-free conditions) will systematically introduce a positive or negative

(here positive) bias in the variable that is averaged (here divergence) if this variable is statistically correlated with the chosen condition. The positive bias arises because rain and surface divergence are not dynamically independent. Hence the sign of the conditionally averaged divergence is not necessarily meaningful.

b. Toy model

A toy model is proposed below with the purpose of illustrating how a conditional average can shift the values of divergence towards positive or negative values, suggesting a different interpretation of ON17's figures. In the present case, our toy model is constructed such that a stationary, weak convergence coexists with random fluctuations that dominate the signal at any time but do not impact the long-term average. This toy model mimics two physical properties of the fields that are considered:

1. Rain and surface divergence are not independent variables: convective rain events are associated with mesoscale motions which include strong convergence roughly beneath the precipitating cell.

2. In the boundary layer, over a sufficiently long time and over a wide enough region, there is no net export or import of air. In other terms, strong convergence must be compensated by divergence in other locations.

The toy model describes the divergence spatial field, assuming that it consists of a permanent feature and random fluctuations that resemble convective events (rain associated to strong convergence values). To simplify we consider only one-dimensional signals, noted $d(y,t)$, where y is a spatial dimension (e.g. transverse to a front of Sea Surface Temperature) and t is time. We assume that the divergence field is the sum of a permanent component, $d_p(y)$, and fluctuations $d_s(y,\ t)$

composed on several individual "storms" at each time, centered at random locations $y_c(t)$, but all with the same spatial shape (see Appendix),

$$d(y,t) = d_p(y) + d_s(y,\, t)\ . \tag{1}$$

Note that, no assumption on the physical origin of the permanent signal is required in the following development as we only want to stress out difficulties in interpreting conditional averages.

We also consider that, at any particular time, d_p and d_s integrate to zero over the domain of interest and that storms d_s occur at random locations with uniform probability so that they cancel out in the long run. In this case, the time-averaged divergence yields $d_p(y)$:

$$\overline{d}(y) = \frac{1}{T}\int_0^T d(y,t')\,dt' \rightarrow d_p(y)\ . \tag{2}$$

Using simple sinusoidal functions, an implementation has been carried out, details are given in the Appendix. For simplicity, at each timestep, 5 "storm" centers are defined at random (uniformly distributed) locations in the domain (of length $2\times D = 5000$ km). Each storm consists in a region of convergence of maximal magnitude $a = 1.0\times 10^{-4}\,\mathrm{s}^{-1}$ and of width $2\times l = 100$ km, compensated by weaker divergence of maximal magnitude $1.0\times 10^{-5}\,\mathrm{s}^{-1}$ and over a width $L = 500$ km on both sides. The stationary signal has a smaller magnitude, of $0.5\times 10^{-5}\,\mathrm{s}^{-1}$. Figure 1 illustrates the stationary signal (panel a) and a typical instantaneous divergence field (panel b). It confirms that the stationary signal is dwarfed at any time by the intermittent signal from the fluctuations with much larger amplitude.

In ON17, the conditional average is taken over rain, which is related in some proportion to divergence. To represent this we produce an intermediate field $r(y,t) = -d_s(y,t) + \eta$, where η is a random Gaussian noise (to make the field $r(y,t)$ more similar to rain, one could set all its negative values to zero). The conditional average is then taken using the condition $r > 0$ ('rain only') or $r \leq 0$ ('rain free'). Figure 2a illustrates the resulting averages obtained for different numbers of

timesteps used. In the overall average, the stationary signal $d_p(y)$ is recovered (note that a signal different from d_p is observed near the boundaries of the domain due to a finite domain effect). In the rain-free average, the same signal is recovered but shifted to positive values. The shift is sufficient that all values (even in the region of convergence for $d_p(y)$) become positive. In other words, this shift, or positive bias, is larger than the amplitude of $d_p(y)$. The 'rain-only' signal is shifted to strongly negative values; again the spatial structure is unaltered but it is hidden in the noise unless a long time average is taken.

The conclusion from this figure is that the conditional average (in the setting of this toy model) shifts the 'rain-free' average towards positive values, but without altering its spatial structure. Moreover, as the rain-free average excludes the intense values (tied to storms), it is less noisy than the the overall average. The rain-only average including mainly extreme events is by construction very noisy.

c. The positive bias

We now take advantage of the simplicity of this toy model to quantify, in this case, the amplitude of the positive bias. This can be calculated simply in the case when there is no noise, i.e. we average conditionally on the sign of $d_s(y,t)$ and we consider only one storm by timestep. The storm locations being uniformly distributed and the spatial shape of $d_s(y,t)$ being fixed, the 'rain frequency' $\chi = p(\text{rain} > 0)$ is uniform across the domain and is given by the ratio of the width of the convergent region ($d_s < 0$) over the width of the domain, $2 \times D$, such that $\chi = l/D$. The form given to the convergence is such that its average value computed over the convergence zone is $-2a/\pi$. Hence the rain-only average is

$$\overline{d}^{RO}(y) = d_p(y) - \frac{2a}{\pi}. \tag{3}$$

As all times are partitioned into rain-free and rain-only, one necessarily verifies $\overline{d} = \overline{d}^{RF}(1-\chi) + \overline{d}^{R0}\chi$ and the rain-free average can be calculated as

$$\overline{d}^{RF}(y) = d_p(y) + \frac{2a}{\pi}\frac{l}{D-l}. \tag{4}$$

The above gives an estimate of the systematic biases introduced by the conditional averaging in absence of noise, i.e. when $r(y,t) = -d_s(y,t)$. When a random noise is present, rain and divergence have a less simple relation but are correlated. As the noise increases, the biases decrease in absolute value from their values obtained above, and the asymmetry between rain-free and rain-only means decreases, as illustrated from figure 2b. Nonetheless, because the signature in convergence of the rain events is much larger than that of the stationary signal, $a \gg \max(d_p(y))$, and despite the fact that they occupy a small portion of space ($l/(D-l) \sim l/D \ll 1$), it is likely that the positive bias is sufficient to shift the whole signal of $\overline{d}^{RF}$ to positive values.

The point that the above toy model illustrates is that the absence of convergence in the rain-free conditional average ($\overline{d}^{RF}(y) < 0$) does not rule out the presence of a stationary signal in the divergence field. It merely reflects that divergence and rain are strongly correlated, as illustrated by ON17 (see their figure 4c). We return to this issue below and in section 4.

3. Idealized atmospheric simulation

In order to bridge the gap between the maps displayed by ON17 and the one-dimensional illustrations from our toy model, we here take advantage of a simulation carried out for investigating the atmospheric response to mesoscale Sea Surface Temperature (SST) anomalies. This simulation will be described in a manuscript currently in preparation. It consists of an idealized set-up of a midlatitude storm-track using the Weather Research and Forecast (WRF) Model (Skamarock et al. 2008), in a zonally periodic channel and using a gray radiation scheme (Frierson et al. 2006). The

domain is 9216 km in both horizontal directions, and extends up to about 20 km (50 hPa) in height. The horizontal resolution ($dx = 18$ km) allows a good description of atmospheric storms, leading to a reasonable storm track. Boundary layer processes are represented by the YSU scheme, convection by the Kain and Fritsch scheme, and microphysics by the Kessler scheme. The fixed zonally symmetric SST distribution in the simulation presented here consists of a large-scale meridional gradient with maximal amplitude of 4 K / 100 km. The simulation has been carried out for 4 years and the first 90 days were discarded. Data were recorded every 12h.

a. Conditional averages of surface divergence

Figure 3 shows the rain frequency and the mean rain rate over the whole domain, clearly indicating a preferred location for rain which is south and away from the SST front. This may be compared to Figure 2 of ON17, the comparison suggesting that our simulation has a realistic mean rain rate but overestimates the maximum rain frequency and the meridional contrast in rain frequency over the SST front. This does not matter for the present purpose, which is again to illustrate the systematic bias introduced by the conditional averages and by other similar filters.

Figure 4 shows the time-average and conditional averages of the surface divergence, as in Figure 1 of ON17. The mean surface divergence (panel a) shows a pattern with convergence South of the SST front, and divergence over the SST front and to the North of it, analogous to that displayed over the Gulf Stream by ON17. Mean values (extremes of about $\pm 0.4 \times 10^{-5}\,\mathrm{s}^{-1}$) are quite comparable with the values found from observations. For the conditional averages, as expected, the rain-free divergence is shifted to positive values in all locations (panel b), whereas the rain-only divergence is shifted to only negative values (panel c).

Now, one advantage of this idealized setting is the zonal symmetry of the underlying SST, allowing to average easily in the along-front direction. This averaging leads to the same presentation as

for the toy model of section 2. Figure 5 shows the zonally averaged time-mean surface divergence, along with the rain-free and rain-only conditional averages. In addition, the underlying Laplacian of SST is also displayed as an indication of area where surface convergence is expected in the EBMA theory. Again, it is clearly seen that the conditional average displaces the rain-free average to positive values, the rain-only average to negative values. Both conditional averages retain some of the spatial structure present in the all-weather average, but there are also notable differences. For example, in the rain-free average the central couplet occurs on shorter spatial scales than in the all-weather average. The meaning and interpretation of these differences is not the purpose of the present comment, and would anyhow be tied to specificities of these idealized simulations. The important message is that the conditional average of divergence, conditioned on a variable with which divergence is correlated, leads to a bias which makes the convergent values disappear from the rain-free average. The disappearance of these convergent values does not allow the interpretation made by ON17, i.e. that a stationary (or permanent or persistent) feature be absent from the divergence field.

The same simulation can be used to illustrate another analysis made by ON17, bearing on the statistics of divergence. The skewness of the divergence distribution was emphasized as a crucial parameter (e.g. section 6 of ON17). As a complement to the conditional averages, ON17 examined the average of divergence when extreme values (away from the mean by more than twice the standard deviation) are excluded, or when only extreme values are retained (ON17, figure 5). This was not explored in the toy model because the distribution of divergent values in there was not tied to a physical description of the processes. In the numerical simulation with a mesoscale model it becomes meaningful to explore this distribution. Figure 6 shows maps of the mean divergence overall and filtered divergence excluding extreme values or retaining only those. The format for the first four panels is the same as that of figure 5 of ON17. As shown by panel d, the $2 \times \sigma$ filter

removes a comparable amount of data (4 to 5%) in the area of maximum convergence. Again, the maps are very similar to the rain-free and rain-only means. In particular, the mean divergence excluding extreme values (Fig. 6b) is positive essentially everywhere, as the rain-free mean (Fig. 4b). Yet, as we saw previously it is not the sign of the mean divergence that is meaningful, but the spatial variations: in both cases the rain-free divergence did retain conspicuously part of the spatial variations present in the overall time-mean. In the last two panels of figure 6 (bottom row), the averaged divergences excluding or retaining extreme values are presented, but removing their domain average. It then becomes apparent that the former includes spatial variations very similar to those of the mean divergence, but slightly weaker. In contrast, the mean including only extreme events consists only of a strong band of convergence, wider than that of the overall mean divergence, and without the positive counterpart to the North. These different spatial structures and relative amplitudes can be better appreciated from the zonally averaged description of these means in figure 7, rather than in maps where the choice of colors guides the eye and interpretation. It would be very informative in ON17 if their figures 1 and 5 were complemented with similar figures: for example, instead of presenting only the rain-free mean divergence, if a panel was included to show the rain-free mean divergence minus the spatial average over the area shown. Alternatively, the rain-free divergence could be shown with contours overlaid to the overall mean divergence, so one could see if the spatial variations and features coincide (but the comparison of the amplitudes would remain difficult).

b. Statistics of divergence values

Finally, we use the simulation to explore the overall distribution of the values taken by the divergence, similar to ON17 in their figure 6. The distribution of divergent values in our simulation is shown in figure 8a, showing good qualitative agreement with the distribution displayed from

observations by ON17. In particular, we also find that large positive values of divergence are more frequent in rain-only conditions than in rain-free conditions, implying that there is not systematically convergence below rain. But we emphasize that the large positive values are *one order of magnitude less likely than negative values*. Now it was stressed several times above that divergence and rain are not dynamically independent, and that they are statistically correlated. The simulation allows to document the joint Probability Distribution Function of divergence and rain, shown in figure 8b. The mean divergence, for a given value of rain, is negative and increasingly negative as the rain value increases, as shown by the blue line. This gives another *a posteriori* justification of the set-up of the toy model, where the intermediate rain field has been built by adding random noise to the divergence. This also allows to revisit how the sign of the rain-only mean divergence is determined. If we write $p(e)\,de$ the probability that the divergence takes a value between e and $e+de$, the overall mean divergence can be written:

$$\overline{d} = \int_{-\infty}^{\infty} e\,p(e)\,de\,, \tag{5}$$

The rain-only mean divergence (calculating using only values of rain above a threshold ε) is then written

$$\overline{d}^{RO} = \frac{\int_{-\infty}^{\infty} e\,p(e|\text{rain} > \varepsilon)\,de}{\int_{-\infty}^{\infty} p(e|\text{rain} > \varepsilon)\,de}\,. \tag{6}$$

In the integrand of the numerator in equation (6), one may decompose the conditional probability on rain being larger than the threshold ε, and write it as the sum of the conditional probabilities knowing that rain is within interval $[r, r+dr[$:

$$e\,p(e|\text{rain} > \varepsilon) = \int_{\varepsilon}^{+\infty} e\,p(e|r \leq \text{rain} < r+dr)q(r)\,dr\,. \tag{7}$$

with $q(r)$ the probability density function for the rain rate. This yields

$$\begin{aligned}\overline{d}^{RO} &= \frac{\int_{-\infty}^{\infty} e \int_{\varepsilon}^{+\infty} e\, p(e|r \leq \text{rain} < r+dr) q(r)\, dr\, de}{\int_{-\infty}^{\infty} p(e|\text{rain} > \varepsilon)\, de} \\ &= \frac{\int_{\varepsilon}^{+\infty} q(r) \int_{-\infty}^{+\infty} e\, p(e|r \leq \text{rain} < r+dr)\, de\, dr}{P(rain > \varepsilon)} \\ &= \frac{\int_{\varepsilon}^{+\infty} q(r) \lceil(r)\, dr}{P(rain > \varepsilon)} \end{aligned} \tag{8}$$

with $\lceil(r) = \int_{-\infty}^{+\infty} e\, p(e|r \leq \text{rain} < r+dr)\, de$. Up to a normalizing factor, $\lceil(r)$ is the average divergence knowing the rain rate. This is calculated in our simulations and shown in figure 8b as the thick blue line. Consistent with the physical expectation that surface convergence and precipitation are highly correlated, the average divergence knowing the rain rate is always negative for values of rain larger than about 1 mm/day, and increasingly negative with increasing precipitation. This clearly demonstrates that the correlation of convergence and precipitation leads to $\overline{d}^{RO}$ being negative. In consequence $\overline{d}^{RF}$ will systematically have a positive shift relative to $\overline{d}$. Note that, because strong convergence corresponds to rain-only regions (see Fig. 8a), an analysis based on the 2σ filter would lead to the same conclusion. The reason is that the condition still is strongly correlated to the divergence itself.

4. Discussion and perspectives

ON17 conclude from their analysis *'that the existence of the GSCZ in the time-mean winds owes its existence to extreme storm convergences, since removing a relatively small number of data points associated with storms removes the time-mean convergence'* (section 3f, p2397). In the conclusion again they state that *'strong convergences associated with storms explains the existence of the GSCZ in the time-mean winds'* (section 6, p2409). They explain that the skewness of the surface divergence distribution, due to the strong convergence signatures of mid-latitude cyclones, *'is sufficient to change the sign of the time mean and the interpretation of the SST influence on*

divergence. Removing fewer than 4% of the strongest divergence events, or removing fewer than 20% of values in raining conditions, effectively eliminates the GSCZ from the time-mean surface winds' (section 6, p2409). The underlying premise is that, if the convergence band vanishes when only a small portion of values are removed, this feature cannot be *'a persistent feature anchored to the Gulf Stream'* (section 4d, p2404).

We disagree with this premise, but this does not invalidate the entire analysis of ON17 and their conclusions. Our disagreement stems from the too strong emphasis on the sign of the rain-free divergence. Our study has put in evidence the bias in this sign because of a dynamical link between surface divergence and precipitation that statistically correlates the two fields. As a consequence, the conditional average shifts the rain-free divergence towards positive values and the rain-only divergence towards strongly negative values. The correlation between precipitation and surface divergence is especially true for the most intense values as can be seen in their figures 4b and 4c. The joint PDF of convergence and precipitation, as shown in figure 8b for our simulations, illustrates clearly this correlation. It would be very interesting to estimate this joint PDF from observations. Yet, as far as the color bars in their Figure 1, 5, and 13 allow to judge, much of the spatial variations between the rain-free and all weather divergence coincide. Rather than showing the absolute values of the rain-free and rain-only divergence, showing anomalies (relative either to the mean over the domain, or to the field smoothed on large scales) would be less misleading. In the case of the toy-model, the same spatial structure came out in the three averages, but the rain-only average is noisier. In the idealized simulations, the spatial structures of the rain-free average has strong resemblance to those of the overall average, whereas those of the rain-only average display some differences.

In the comparisons of their different figures, ON17 emphasize absolute values and discard the similarity that is often found between the spatial variations. For example, the claim of ON17 that

the rain-free divergence in their figure 13b *'bears no resemblance'* (p2401) with the SST Laplacian (figure 13h) is at the very least misleading. The spatial variations of both fields, as far as eye can tell, seem very correlated. The colors differ because the rain-free divergence is shifted everywhere to positive values because of the conditional average. Similarly, in the interpretation of their figure 11, the strong similarity at spatial scales less than 1000 km (panels 11a and 11b) is perhaps more significant than the difference in the worth emphasizing than the difference (again a positive shift) in the spatially lowpass-filtered fields (panels 11c and 11d).

it is worth emphasizing that on spatial scales less than 1000 km (panels 11a and 11b), there is a strong similarity between the time-mean divergence (colors) and the SST Laplacian (contours).

Now, to make progress we suggest to make the line of reasoning of ON17 more explicit, and to formulate two different hypotheses:

1. **H1**. The divergence at any time results from two signals: a stationary signal (related to EBMA), and random fluctuations from storms whose positions vary in time. The signal due to these fluctuations should diminish when averaging over longer times.

2. **H2**. The divergence at any time only results from storms. The spatial variations of these storms are such that in the time-average they produce the signature that is observed.

Set in the above terms, ON17 claims that the absence of convergence (negative values) in the rain-free average divergence rules out hypothesis **H1**. The toy model of section 2 merely served to illustrate that this conclusion is not justified: it is *possible* to have a rain-free divergence everywhere positive and yet to have a stationary signal which is responsible for all of the time-averaged signal. In other words, the absence of *convergence* in the rain-free divergence (or after filtering out extreme values) does not rule out **H1**, i.e. the existence of a permanent signal in the divergence.

Now, in our toy model, the shift is uniform in space as the storms were uniformly distributed in space. In contrast to this, in our idealized simulation (see section 3) and in the observations (see panel c of figure 1 of ON17) the shift is not uniform. Introducing spatial variations in the probability of occurrence of the storms in our toy model (see Appendix for description of the modifications of the toy model), one observes that storms still leave a residual signal that is related to the stationary divergence term (Fig. 9). Of course, this is on top on another signal due to the localization in space of storms in relation with **H2**.

Spelling out explicitly the two hypotheses provides two extreme pictures, and reality is likely, as often, in between. The links between the conditional averages analyzed by ON17 and the underlying mechanisms of the atmospheric response to the SST anomalies are not so simple, as illustrated by the present comment. Now, the detailed and extensive analysis carried out by ON17 does emphasize several important points: the instantaneous fluctuations in the divergence field overwhelms the time-mean, and understanding this response requires to consider how the SST influences storms, in particular in setting their preferred location. We believe that detailed investigations of the instantaneous signature of different mechanisms through which the SST influences the marine atmospheric boundary layer, as sketched in section 5 of ON17, are necessary to properly evaluate the relevance of these different mechanisms. These issues are complex as they depend on the variables and approach considered to quantify one or other mechanism, as will be discussed based on the simulations used in section 3 (Foussard et al, manuscript in preparation).

Acknowledgments. This work was granted access to the HPC resources of IDRIS under the allocation for 2015 and 2016 A0020106852 made by GENCI (Grand Equipement National de Calcul Intensif).

APPENDIX

Implementation of the toy model

The toy model we constructed only depends on the divergence fields d_p and d_s. We here describe the choices used to implement it. The permanent divergence signal was chosen as

$$\begin{aligned} d_p(y) &= A \sin\left(\frac{\pi y}{2L}\right), \quad \text{for} \quad -2L < y < 2L, \\ &= 0, \quad \text{for} \quad |y| > 2L, \end{aligned} \tag{A1}$$

The divergence field is constructed as a sum of d_p and of 5 'storms', each centered at a random (uniformly distributed) location within the domain $[-D, D]$. Each event, relative to its central location, has the following spatial structure:

$$\begin{aligned} g(y) &= \frac{a\,l}{L} \sin\left(\frac{(y+l)\,\pi}{L}\right), \quad \text{for} \quad -(L+l) < y < -l, \\ &= -a \cos\left(\frac{y\,\pi}{2\,l}\right), \quad \text{for} \quad -l < y < l, \\ &= \frac{a\,l}{L} \sin\left(\frac{(y-l)\,\pi}{L}\right), \quad \text{for} \quad l < y < L+l, \\ &= 0, \quad \text{for} \quad |y| > L+l, \end{aligned} \tag{A2}$$

where $-a$ describes the peak intensity of the convergence ($a > 0$), where l describes the width of the convergent region, and L describes the width of the surrounding regions where compensating divergence occurs. This definition is consistent with our idea that the net divergence would be zero (i.e. $\int g(y)dy = 0$). Then d_s takes the form of

$$d_s(y,t) = \sum_{i=1}^{5} g(y - y_c^i(t)) \tag{A3}$$

where $y_c^i(t)$ is the location of one of the storm centers at time t.

In order to obtain the 'rain' field $r(y,t) = -d_s + \eta$, a random noise η is added. This noise has normal distribution with zero mean and a standard deviation of σ_{noise}.

The values chosen for the parameters in order to generate the figures were: $A = 0.5 \times 10^{-5}\,\mathrm{s}^{-1}$, $a = 1 \times 10^{-4}\,\mathrm{s}^{-1}$, $l = 50\,\mathrm{km}$, $L = 500\,\mathrm{km}$, and $D = 2500\,\mathrm{km}$. The number of points in the y direction is $ny = 200$. Different values for the parameters have been explored. As the noise is increased, the positive bias of the rain-free mean divergence decreases. Nonetheless, as long as the noise is not much larger than a, the positive bias is robust and significant (i.e. sufficient for the rain-free mean to be positive nearly everywhere).

The model was also modified to show that the same results can be obtain when storms are located on the convergence zone. To this end we introduce a parameter $0 < C < 1$. For each event, we take two random numbers, r uniformly distributed in $[0,\ 1[$ and s with a Gaussian distribution (centered at 0, and with variance 1). The storm position y_c is then defined as

$$\begin{aligned} y_p &= (1-s)L \quad \text{if} \quad r < C, \\ &= \left(2\frac{r-C}{1-C} - 1\right) D \quad \text{if} \quad r \geq C \end{aligned} \tag{A4}$$

Figure 9 was produced with this scheme, still using 5 storms by time step, but without noise ($\sigma_{noise} = 0$) and with 10000 timesteps. Parameter C was set to $C = 0.4$. The other parameters were the same as before.

References

Bryan, F. O., R. Tomas, J. Dennis, D. Chelton, N. Loeb, and J. McClean, 2010: Frontal scale air-sea interaction in high-resolution coupled climate models. *J. Climate*, **23**, 6278–6291.

Businger, J. A., and W. J. Shaw, 1984: The response of the marine boundary layer to mesoscale variations in sea-surface temperature. *Dyn. Atmos. Ocean*, **8**, 267–281.

Butchart, N., 2014: The Brewer-Dobson circulation. *Rev. Geophys.*, **52**, 157–184.

Chelton, D. B., M. G. Schlax, M. H. Freilich, and R. F. Milliff, 2004: Satellite measurements reveal persistent small-scale features in ocean winds. *Science*, **303**, 978–983.

Feliks, Y., M. Ghil, and E. Simonnet, 2004: Low-frequency variability in the midlatitude atmosphere induced by an oceanic thermal front. *J. Atmos. Sci.*, **61**, 961–981.

Frierson, D. M., I. M. Held, and P. Zurita-Gotor, 2006: A gray-radiation aquaplanet moist GCM. Part I: Static stability and eddy scale. *J. Atmos. Sci.*, **63**, 2548–2566.

Hayes, S. P., M. J. McPhaden, and J. M. Wallace, 1989: The influence of sea surface temperature on surface wind in the eastern equatorial Pacific: weekly to monthly variability. *J. Climate*, **2**, 1500–1506.

Lambaerts, J., G. Lapeyre, R. Plougonven, and P. Klein, 2013: Atmospheric response to sea surface temperature mesoscale structures. *J. Geophys. Res.*, **118**, 9611–9621, doi:10.1002/jgrd.50769.

Lindzen, R., and S. Nigam, 1987: On the role of sea surface temperature gradients in forcing low-level winds and convergence in the tropics. *J. Atm. Sci.*, **44**, 2418–2436.

Minobe, S., A. Kuwano-Yoshida, N. Komori, S.-P. Xie, and R. J. Small, 2008: Influence of the Gulf Stream on the troposphere. *Nature*, **452**, 206–209.

O'Neill, L. W., T. Haack, D. B. Chelton, and E. Skyllingstad, 2017: The Gulf Stream Convergence Zone in the time-mean winds. *J. Atm. Sci.*, **74**, 2383–2412.

Skamarock, W., and Coauthors, 2008: A description of the Advanced Research WRF Version 3. *NCAR Technical Note*.

Small, R., and Coauthors, 2008: Air–sea interaction over ocean fronts and eddies. *Dyn. Atmos. Oceans*, **45**, 274–319.

LIST OF FIGURES

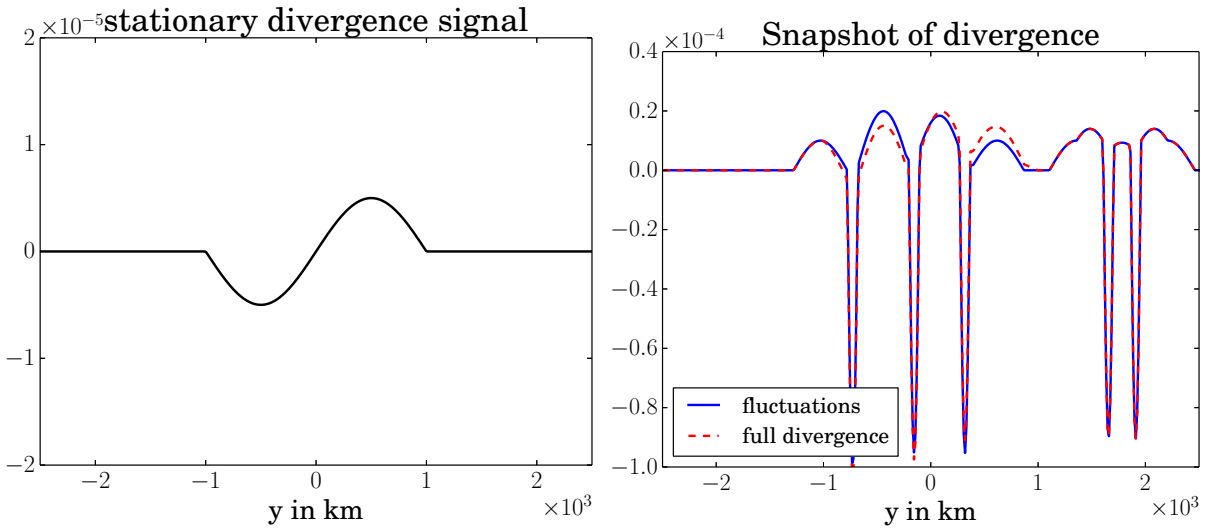

FIG. 1. (a) The stationary divergence $d_p(y)$ (in s^{-1}). (b) Snapshot of the fluctuating component $d_s(y,t)$ in s^{-1} (blue line) and of the resulting full divergence signal $d(y,t)$ (red, dashed line). Note the different vertical scale relative to (a).

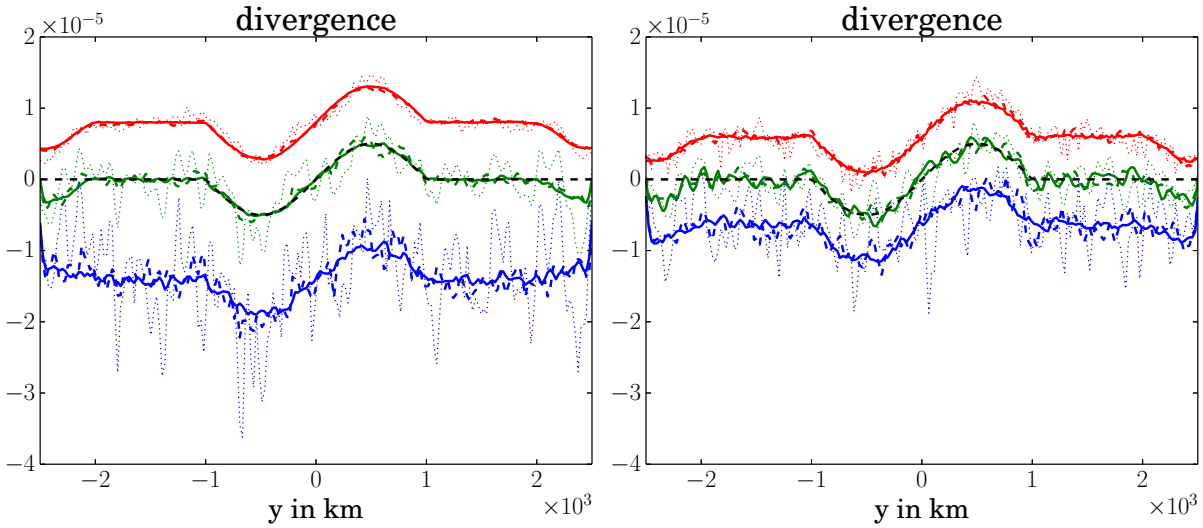

FIG. 2. (a) Time-mean divergence of the toy model, averaged over 10000 timesteps (thick lines), over 1000 timesteps (dashed lines) and 100 timesteps (dotted lines). The green lines correspond to total averages, whereas the blue lines correspond to *rain-only* and red lines correspond to *rain-free* conditional averages. (b) Same as (a), but with a noise level of $\sigma = 5 \times 10^{-5}\,\mathrm{s}^{-1}$ instead of $1 \times 10^{-5}\,\mathrm{s}^{-1}$. In both panels, the black dashed curve is d_p. Parameters used for the toy model are given in the Appendix.

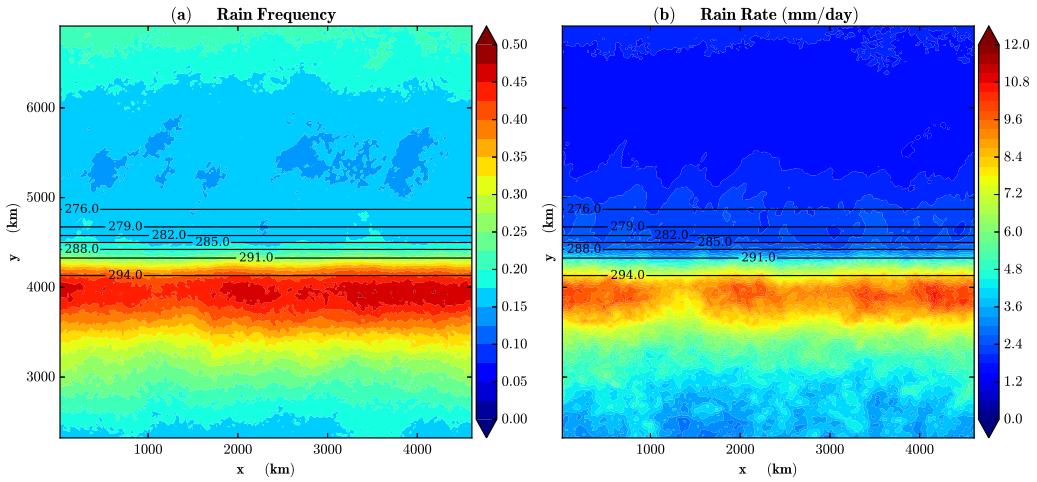

FIG. 3. Mean rain frequency and mean rain rate (in mm/day) over the 4 years. Contours show the SST field in K. All calculations have been made considering rain rates over 12h superior to 3 mm/day.

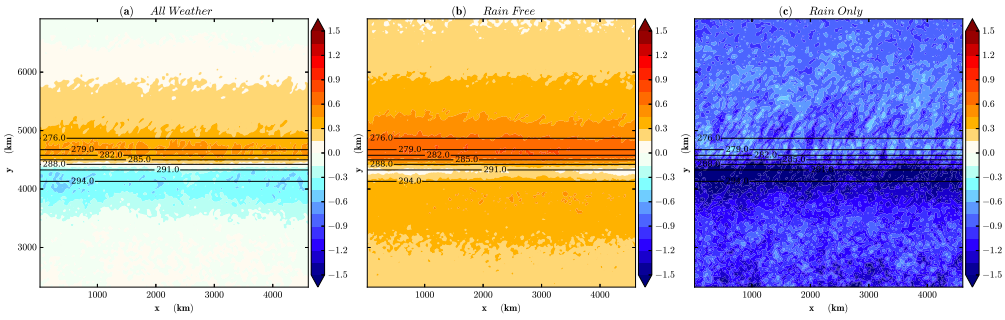

457 FIG. 4. Surface divergence, in colors and in 10^{-5} s^{-1}, considering : (a) unconditional mean, (b) rain-free
458 conditional mean (c) rain-only conditional mean. Contours show the SST field in °C.

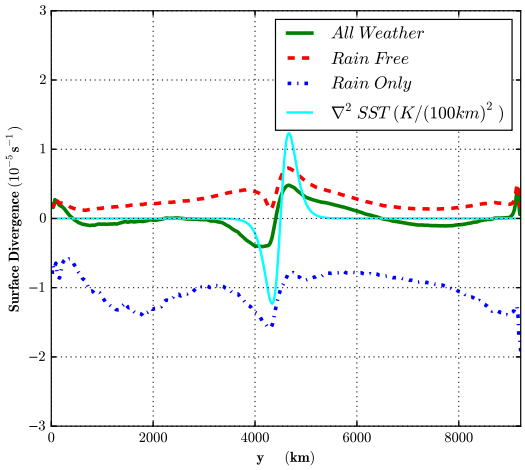

459 FIG. 5. Zonally averaged unconditional and conditional mean of surface divergence in 10^{-5} s^{-1}. Same
460 quantities as for panels (a), (b) and (c) of Fig. 4, considering the zonal mean of the signals. The light blue line is
461 the Laplacian of SST in 10^{-10} K m^{-2}.

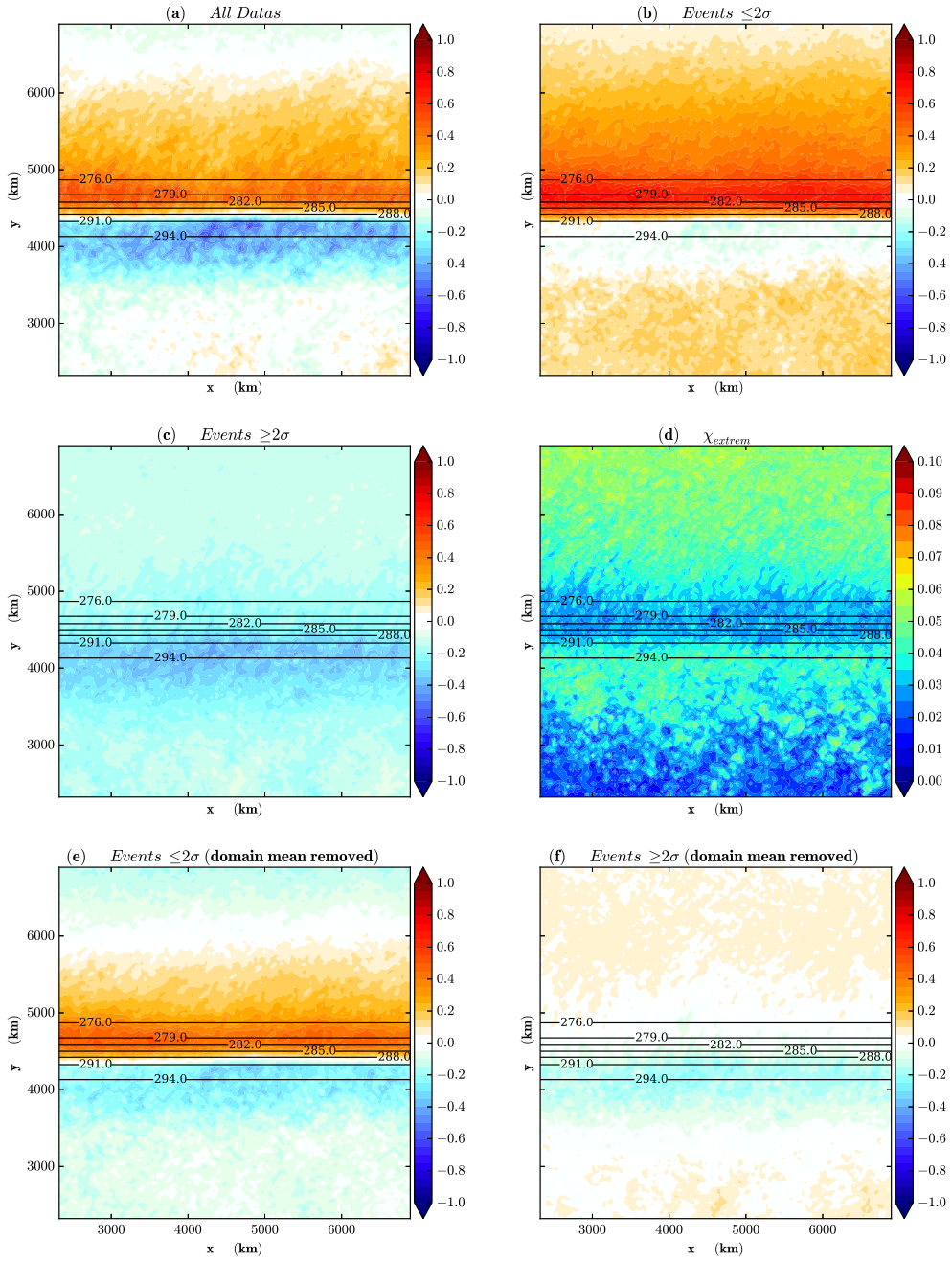

462 FIG. 6. Mean Surface divergence, in shadings and in 10^{-5} s^{-1}. (a) for the whole time series, (b) with values
463 smaller than $2 \times \sigma$, (c) with only values larger than $2 \times \sigma$. (d) percentage of points with deviation from the mean
464 bigger than the $2 \times \sigma$ threshold. (e-f): Same as (b-c) after subtracting the domain-averaged signal. Contours
465 show the SST field in K.

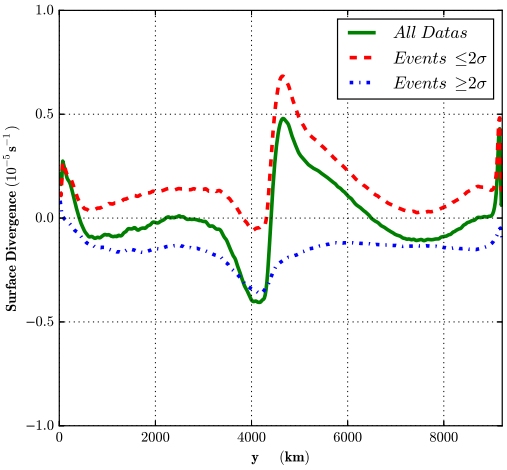

466 FIG. 7. Unfiltered and filtered surface divergence in 10^{-5} s^{-1}. Same quantities as for panels (a), (b) and (c)
467 of Fig. 6, considering the zonal mean of the signals.

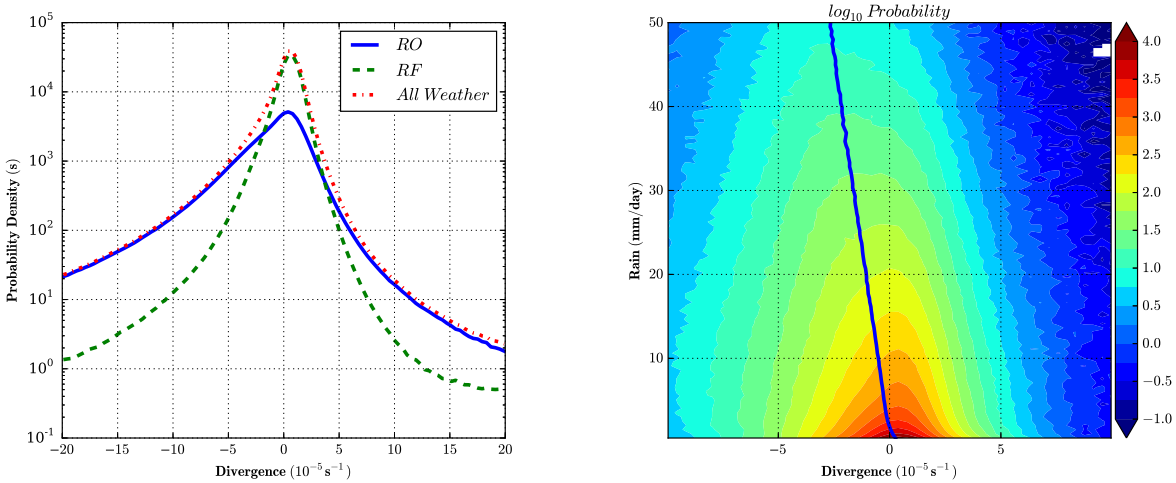

FIG. 8. (a) Probability density function of the surface divergence (red curve), calculated from all time outputs and for points within a band of latitudes (3600 km $\leq$ y $\leq$ 5600 km). Blue and green dashed lines show respective contributions of the rainy and rain-free points to the unconditional PDF. (b) Joint probability density function of the rain rate (vertical axis, in mm/day) and the surface divergence (horizontal axis, in 10^{-5} s^{-1}). Color scale is logarithmic. The blue line indicates the conditional mean of the surface divergence for a given rain rate.

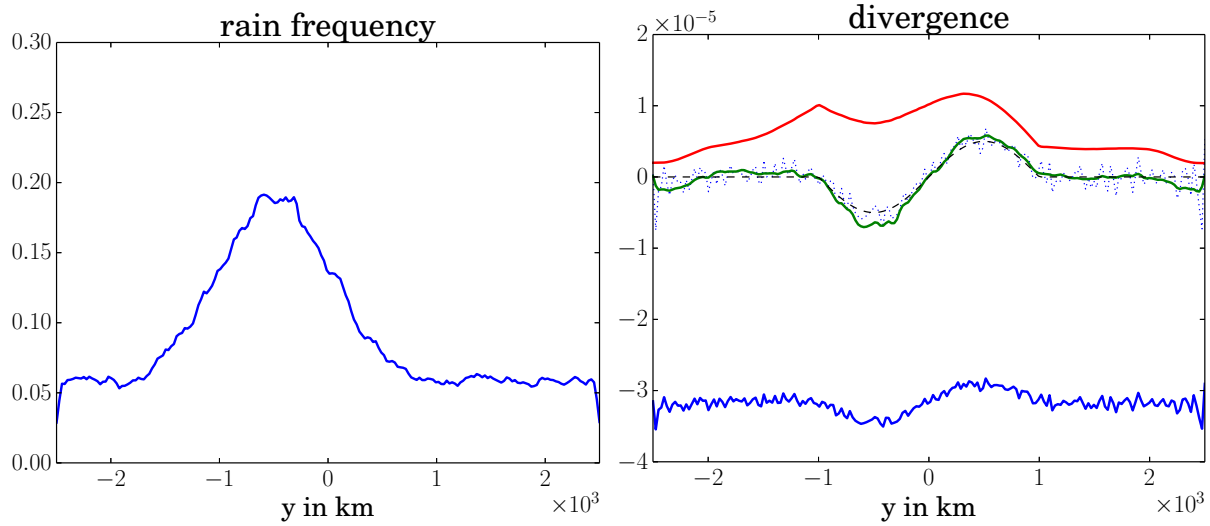

FIG. 9. (a) Rain frequency for the modified toy model. (b) Time-mean divergence of the modified toy model, averaged over 10000 timesteps. The green line correspond to total averages, whereas the blue line correspond to $\overline{d}_{RO}/2$, the red line to $\overline{d}^{RF}$ and the dashed black line to d_p. The blue dotted curve is $\overline{d}_{RO}$ minus its spatial average value. It overlaps almost exactly with d_p. Parameters used for the toy model are given in the Appendix.